GEOPHYSICS, VOL. 85, NO. 3 (MAY-JUNE 2020); P. P27–P36, 14 FIGS.
10.1190/GEO2019-0768.1

DOI:10.1190/geo2019-0768.1

Comparing the broadband acoustic frequency response of single, clustered, and arrays of marine air guns

Martin Landrø[1] and Jan Langhammer[2]

ABSTRACT

Field data acquired from a seismic vessel by a seabed hydrophone is used to analyze the broadband response (10 Hz to 62.5 kHz) for various source configurations: single air guns, clustered air guns, and a full array consisting of 30 air guns. The various parts of the acoustic signal are analyzed in detail, and it is found that a high-frequency signal arriving prior to the main peak of a single air-gun signal most likely is caused by small vapor cavities collapsing at or close to the surface of the gun. This is confirmed by high-speed photographs taken when a small air gun is fired in a water tank. When the full array is used, a second type of cavitation signal is observed: ghost cavitation caused by acoustic stimulation by the negative pressure that is backscattered from the free surface. As this ghost signal from 30 different guns arrives at a specific location in the water, cavities might be formed, and they create a high-frequency acoustic signal.

INTRODUCTION

In this work, we study source signatures of single air guns and a marine air-gun array recorded by a far-field hydrophone with a frequency bandwidth of 10 Hz to 62.5 kHz. Originally, the hydrophone has been oriented vertically below the source at the seabed. Traditionally, the primary interest in air-gun performance has been for modeling and measuring the emitted acoustic signals within the seismic bandwidth between 5 and 250 Hz. For marine seismic acquisition, air guns are the most commonly used sources. A brief introduction to air guns can be found in Dragoset (2000). The first example of air-gun modeling was presented by Ziolkowski (1970). Later examples of modeling of air guns can be found in Landrø (1992) and Barker and Landrø (2014).

Recently, interest in high-frequency signals produced by air-gun arrays has increased (Goold and Fish, 1998; Breitzke et al., 2008; Amundsen and Landrø, 2011a, 2011b). Amundsen and Landrø (2010) discuss and present hearing curves of marine mammals. Dolphins and white whales have excellent hearing capacity for frequencies between 10 and 100 kHz. Groenaas et al. (2011) suggest including a high-frequency streamer section in a normal streamer for the purpose of detecting marine mammals. Southall et al. (2019) provide an update of their recommendations for residual hearing effects related to marine mammals; they present estimated group hearing audiograms for high-frequency cetaceans, sirenians, marine carnivores, and low-frequency cetaceans. It is beyond the scope of this work to present detailed comparisons of these hearing curves, but it is certainly interesting to compare the signals emitted by air-gun arrays to the presented hearing curves.

Landrø et al. (2011) discuss the frequency properties and possible causes for the high-frequency signals. They suggest that the mechanism of ghost cavitation can cause a significant amount of high-frequency signals emitted from an air-gun array. The more guns and the closer they are, the more the ghost cavitation effect will contribute to the high-frequency signals. Landrø et al. (2013) discuss repeatability issues related to these signals and conclude that the amount and the timing related to the main peak are repeatable. Khodabandeloo et al. (2017) and Khodabandeloo and Landrø (2018, 2019) demonstrate that these ghost cavities are observable on high-speed video recordings and how these might be included as a time-variant medium when modeling the source signatures. This might have an effect on near-field hydrophone measurements and, more specifically, when such measurements are used to estimate far-field source signatures. These hydrophones record data close to single guns and clusters on the arrays and are now widely used during seismic acquisition for calculating the far-field signatures that again are used in source signature deconvolution during processing; see, for in-

Manuscript received by the Editor 26 November 2019; revised manuscript received 21 January 2020; published ahead of production 11 February 2020; published online 31 March 2020.
[1]Norwegian University of Science and Technology, Department of Electronic Systems, Trondheim, Norway. E-mail: martin.landro@ntnu.no (corresponding author).
[2]TGS, Asker, Norway. E-mail: jan.langhammer@tgs.com.

DOI:10.1190/geo2019-0768.1

stance, Telling et al. (2019). The more we know about the physics in connection with the firing of air-gun sources, the greater confidence we can put into the validity of exploiting near-field measurements for broadband source estimation and deghosting. In addition, such knowledge will help us to design more environmentally friendly air-gun sources and optimize the signal toward the seismic band of interest. In that respect, Watson et al. (2019) focus on the initial peak in their investigation on how physics and source parameters influence the signature of an air gun.

Christie et al. (2019) clearly demonstrate that a secondary "cavity source" can be assigned as an extra notional source. They estimate the position and strength of this source from near-field hydrophone data and show that the difference on the vertical far-field signature is fairly low. This is in good agreement with similar modeling of ghost cavitation performed by Khodabandeloo and Landrø (2019). It is evident from all of these papers (Christie et al., 2019; Khodabandeloo and Landrø, 2019; Telling et al., 2019) that ghost cavitation will reduce the ghost amplitude; therefore, it will indirectly influence broadband source deghosting. Furthermore, we observe that the very first peak of the shoulder signal has approximately the same amplitude (occurring at approximately 44.5 ms for the 300 in^3 air gun and 46 ms for the 70 in^3 air gun) (Figure 5). This observation indicates that the very first peak of the shoulder signal (and the acoustic signature of an air gun) is caused by the solenoid.

Studying the behavior of single guns, clusters of guns, and comparing this to larger source arrays has also gained additional relevance due to new firing techniques introduced to the industry. Abma and Ross (2013) introduce popcorn shooting, allowing the firing time of individual guns to vary over a time period and using sparse inversion for signal reconstruction. Hegna et al. (2018) propose a method for producing a continuous wavefield by spreading the energy emitted from sources out in time. The method of not firing all of the guns in a source array simultaneously, but activating them in a continuous firing scheme, may allow for increased vessel speed and efficiency. This way of firing air guns also claims to be more environmentally friendly due to lower instantaneous sound pressure levels (SPLs). However, in the future, these new firing techniques also will be subject to more investigations with respect to their impact on marine life.

In this paper, the focus is on how single air guns contribute to the high-frequency signals produced, and how the high-frequency signals emitted by single guns compare to those of a large air-gun array. What are the mechanisms behind such effects, and how strong are the high-frequency signals from single air guns compared with those from a compact full array of guns? Can we use superposition and assume that the amount of high-frequency signal created by a full array is the sum of the amounts of each individual gun? The ghost cavitation hypothesis does not support such a linear superposition because the ghost cavitation mechanism is nonlinear: It requires the ghost signal to be greater than a certain threshold before it is activated. In other words, an array of three or four small air guns might not produce ghost cavitation signals at all, in contrast to a larger array. Recently, Coste et al. (2014) present a new air gun in which the amount of high-frequency signals is attenuated. By changing the design of the air gun, they manage to reduce the signal between 100 Hz and 6 kHz by approximately 10 dB. From 7 to 10 kHz, the new air-gun spectrum is slightly above the conventional, but essentially there are no major differences between the new and the conventional air gun at greater than 7 kHz. In this paper, we will discuss conventional air guns only. We analyze and suggest some mechanisms for high-frequency emission from single and multiple air guns used for marine seismic imaging. We find that the amplitude level of the high-frequency signals (at greater than 10 kHz) is small compared with conventional seismic amplitudes, typically 60 dB less.

THE FIELD EXPERIMENT

A field test was performed in the Black Sea offshore Turkey in December 2008. The shooting vessel was the *M/V Marlene Østervold*, and several configurations of the source array were tested. The high-frequency data were recorded by a calibrated omnidirectional electrical broadband TC4033 hydrophone located and anchored at a fixed position at the seafloor. The hydrophone had a usable frequency range of 1 Hz to 140 kHz, with sensitivity of −203 dB relative to 1 V/μPa. The sample rate was set to 0.008 ms, which provides reliable data up to 62.5 kHz (the Nyquist limit).

Several source lines were acquired straight above the hydrophone location, and for each line approximately 40 shots were fired as the source vessel was sailing on a straight line crossing over the sea-bottom hydrophone. The water depth in the area varies between 50 and 60 m. In this paper, we analyze data from four different source configurations: a single 70 in^3 air gun, a single 300 in^3 air gun, a cluster of two 300 in^3 air guns, and the full array (2730 in^3). For the full array, the distance between the gun strings is 6 m and the total number of guns in the array is 30. The source depth is 5 m for all shots used in this paper, and a detailed description of the gun array can be found in Landrø et al. (2013). The precise position of the sea-bottom hydrophone relative to the source array is not known. However, from typical moveout curves, it is possible to find shots that are close to being straight above the hydrophone. For the present analysis, this lack of precise geometry information does not create severe problems. The hydrophone was fixed at the seafloor location when the source vessel traversed the same sail line for several source configurations. This means that the shot positions were repeated and that differences in measured signatures are mainly caused by differences in source configurations (single gun, clustered guns, or full array).

DESIGN OF AIR GUNS AND POSSIBILITIES FOR CAVITY CREATION

Figure 1 shows a small Bolt air gun that has been cut to show the interior of the gun. When the gun is fired, a small amount of air is released from the upper gun chamber and the piston or shuttle starts to move upwards so that air from the lower (and larger) chamber is released through the ports directly into the water surrounding the gun.

The size of the ports of air guns with different volumes is normally the same; one replaces the gun chamber and keeps the rest of the air gun unchanged when the gun volume is changed. A simple and well-known equation often used to describe oscillating cavities or air bubbles is the Rayleigh (1917) equation:

$$R\ddot{R} + \frac{3}{2}\dot{R}^2 = \frac{p_B - p_h}{\rho}, \tag{1}$$

where R is the bubble radius, p_B is the bubble pressure, P_h is the hydrostatic pressure surrounding the bubble, and ρ is the water density. A dot denotes the time derivative. An obvious weakness of equation 1 is that the basic assumption is that the flow is radial and that we assume spherical symmetry. This is not the case when

DOI:10.1190/geo2019-0768.1

compressed air is released through the port openings of an air gun (Figure 1). At the early stages, there are actually four air bubbles (that later merge into one big bubble), and the fluid flow close to these four bubbles is not purely radial. Despite this, the Rayleigh equation gives a reasonable estimate of how the bubble radius and bubble wall velocity vary with time. The probability of cavity creation is closely linked to abrupt changes in water velocity close to the gun. Typically, cavities will form at edges and corners at the gun itself because the largest velocity gradients are likely to occur there. In principle, we expect more cavitation the faster the water initially surrounding the air gun (including the small volume inside the ports) moves outwards. Figure 2 shows a numerical solution of equation 1 assuming that the initial bubble pressure is 137 bar and that the bubble radius is that corresponding to the gun volume. We notice that there is hardly any difference between the maximum bubble wall velocity for the two gun volumes (70 and 300 in^3); hence, we cannot conclude that the larger gun creates more cavities than the smaller gun.

However, if we consider that the air has to escape through narrow ports, the situation is somewhat different. A simple, but far from very accurate, way to model this is to use equation 4 in Landrø et al. (1993):

$$\left[p_0\left(\frac{V_0}{V_0 + Az}\right)^{\gamma} - p_h\right]A = m\ddot{z}, \tag{2}$$

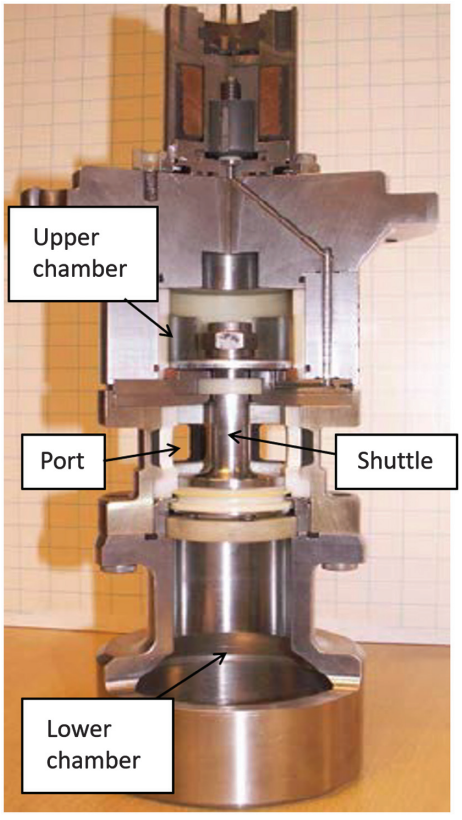

Figure 1. Cutaway model of a small Bolt air gun showing the main chamber (the lower chamber) that initially is filled with compressed air, the upper chamber, the four ports, and the shuttle that moves rapidly upward when the gun is fired.

where p_0 is the initial gun firing pressure, A is the area of the gun port, z is the position of the shuttle, m is the mass of the shuttle, V_0 is the initial gun volume, and γ is the adiabatic constant (1.4 for air). Equation 2 is derived for a water gun, where compressed air is used to push a shuttle so that water is pushed quickly into the seawater, creating big cavities that collapse and create the acoustic signal of a water gun. In our case, we have to assume that the water that is initially in the area between the port openings and the core of the shuttle (Figure 1) escaping through the ports of the air gun acts like a piston on the water that is outside the gun ports. The mass of such a "water piston" is relatively low (probably less than 1 kg), and this number should be divided by four because we have four ports in which this water has to be pushed through at the initial stage after the gun has been fired. Using $m = 0.25$ kg in equation 2 and $A = 0.0005$ m^2, we can estimate the velocity of the water escaping through the ports during the first milliseconds. Because the gun has four ports, we have to correct for this in the volumetric term within the parentheses in equation 2 and modify it to

$$\left[p_0\left(\frac{V_0}{V_0 + 4Az}\right)^{\gamma} - p_h\right]A = m\ddot{z}. \tag{3}$$

Equation 3 describes the motion of a water piston escaping from one port assuming that the mass is equal to the total mass of water that has to be moved out of the gun ports prior to the compressed air. Figure 3 shows the modeled water velocity through the ports using equation 3, and we observe that the largest gun volume gives some-

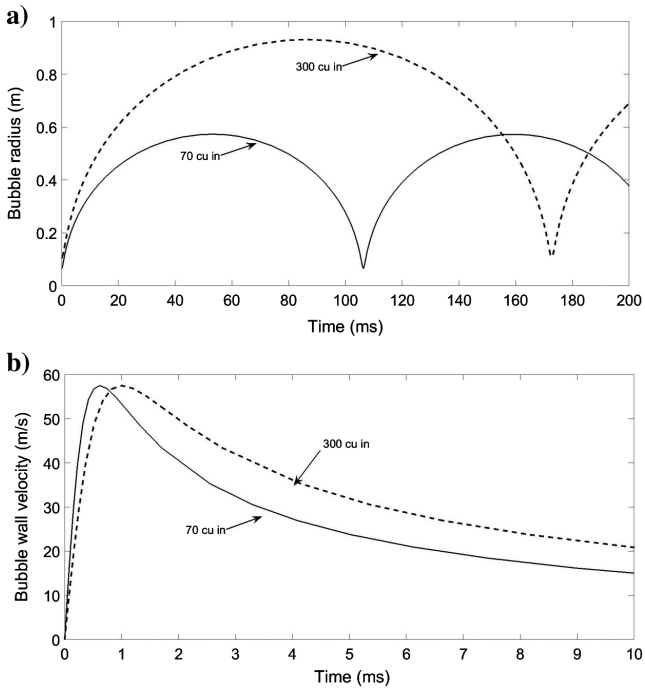

Figure 2. (a) Modeled bubble radius and (b) bubble wall velocity versus time for a 70 (solid line) and a 300 (dashed line) in^3 air gun. These results are obtained by numerical solution of equation 1 (the Rayleigh equation) assuming a source depth of 5 m, and that the initial bubble pressure is 137 bar. As expected, the maximum radius and bubble time period increase with increasing gun volume. In this case, the maximum bubble wall velocity is practically equal for the two gun volumes.

what higher water velocity. In the modeling, the following parameters have been used: $m = 0.25$ kg, $p_0 = 137$ bar $p_h = 1.5$ bar, and $A = 0.0005$ m^2. Both velocities are higher than those estimated directly from the high-speed photography (50 m/s, see the next section). This is reasonable because equation 3 is far from accurate; for instance, there is no friction term, and it is not describing the physics of pushing water through a nozzle correctly. However, it is reasonable to assume that the qualitative difference with respect to volume that is modeled from this equation is correct, and in this paper, this is the main purpose of this equation: to find out whether or not the water velocity will increase with increasing gun volume. An alternative argument supporting higher water velocities for larger gun volumes is that, when the potential energy contained in the lower gun chamber (p_0V_0) increases, there is more energy available to quickly remove the water that is inside the port openings prior to firing the gun. This water has to be removed, and it is very likely that the kinetic energy associated with the motion of this water increases if the potential energy pushing this water increases.

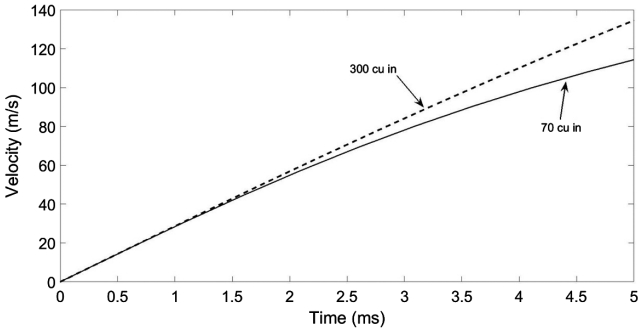

Figure 3. Modeling air escaping through the ports of an air gun using equation 3. Parameters used: $A = 0.0005$ m^2 (port area), $m = 0.25$ kg ("piston mass"), gamma = 1.4, $p_0 = 137$ bar, and $z_s = 5$ m. The larger gun achieves higher water velocity compared with the small gun, indicating the higher probability for cavity creation.

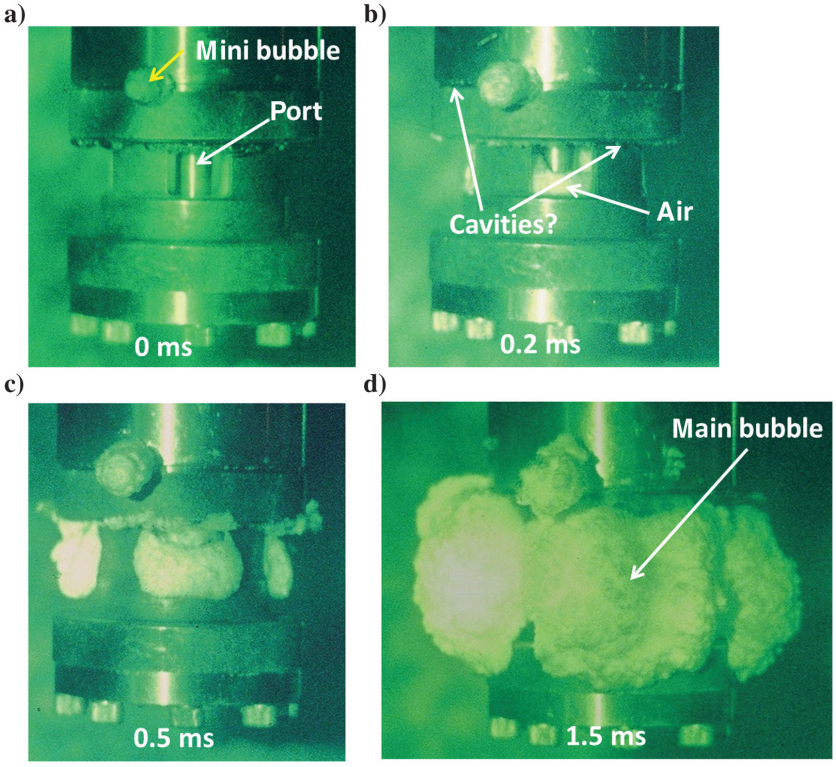

Figure 4. High-speed photos of a 600 Bolt air gun in a water tank. In (a), we see that some air has been released from the upper chamber (the small air bubble marked with a yellow arrow). In (b), the air from the main chamber (the lower chamber) starts to escape through the ports, and (d) clearly shows four bubbles (corresponding to the four ports of the gun) that will merge into one big bubble some milliseconds later (photos from Langhammer, 1994).

HIGH-SPEED PHOTOGRAPHY OF A SMALL AIR GUN IN A TANK

Langhammer and Landrø (1996) present high-speed photographs of a small (1.6 in^3) air gun fired in a water tank. This is the same type of gun that is shown in Figure 1. Figure 4 shows four such photographs taken at various time intervals. In Figure 4a, we observe that there is a small amount of air being released from the upper gun chamber (through a narrow opening in the air gun). This very tiny air bubble is probably causing the "shoulder signal" or precursor of the air-gun acoustic signature. Furthermore, we do not see any sign of the air escaping from the main chamber (the lower chamber) on this photo, which means that the air has not started to move through the ports yet. We also observe some small bubbles attached to the upper ring of the air gun (above the ports). These are probably small air bubbles originating from a small leakage of air from the lower gun chamber. In Figure 4b, we clearly observe that some air is visible inside the gun, ready to escape through the port openings. Here, some of the small bubbles on the upper ring are interpreted as vapor cavities. This is based on visual observation of the high-speed video where these "bubbles" seem to be coupled to the rapid movement of water, and not the slower movement of leaking air bubbles. In Figure 4c, we clearly see that the air has escaped through the ports. This means that the air has moved several centimeters within 0.3 ms (the time interval between Figure 4b and 4c). The distance from the thickness of the port opening is approximately 1 cm, and an estimate of the distance traveled by the air front between these frames is approximately 1.5 cm. A rough estimate for the average velocity of the air-water surface is therefore 0.015 m/0.0003 s = 50 m/s, which is significantly above the threshold for cavity production. Langhammer and Landrø (1996) compare modeled and estimated bubble wall velocities for this small air gun and find similar numbers for the maximum velocity (40 m/s). It should be noted that there are significant uncertainties coupled to this type of velocity estimation. First, there is an uncertainty in the number 0.3 ms (the time delay between frames). The distance traveled has also some uncertainty, although we clearly see from the pictures and direct measurements on the air gun that it is of the order of 1.5 cm. The threshold

DOI:10.1190/geo2019-0768.1

for cavity creation is given as (assuming a depth of 5 m; Landrø et al., 1993)

$$u_c = \sqrt{\frac{2p_h}{\rho}} \approx \sqrt{\frac{3 \cdot 10^5}{10^3}} \text{m/s} = 17.3 \text{ m/s}, \quad (4)$$

which is far below the velocity estimated from the high-speed photography. We note that the threshold velocity increases with depth. This means that it is very likely that cavities are formed close to the air-gun port openings. In Figure 4d, we observe that the four bubbles emerging from each of the four gun ports start to merge and that the size of these bubbles is growing. A rough estimate of the bubble wall velocity based on comparison of Figure 4c and 4d in this series is 2 cm per 0.5 ms corresponding to 40 m/s. Figure 4b shows potential water vapor cavities (marked by the white arrows). Note that these cavities occur on the metal right above the gun ports and not below. A possible explanation for this is that the air is escaping toward the water surface (the piston or shuttle also is moving upward) so the largest water velocities will occur right above the port openings; hence, the cavities will be "glued" to the area right above the port openings. We also notice that there are some cavities on the ring above the port; however, the number of such cavities is less than those in close vicinity to the gun ports. The size of these cavities is (estimated from Figure 4) between 1 and 4 mm. Using Rayleigh's (1917) equation for the collapse time of a cavity, assuming an initial radius $R = 1$ mm, we get

$$\tau = 0.915R\sqrt{\frac{\rho}{p_h}} \approx 0.02 \text{ ms}, \quad (5)$$

which means that these small cavities will collapse within a very short time frame — most likely within less than 0.1 ms.

Another interesting observation from Figure 4 is that the small bubble or minibubble grows at a more moderate speed compared with the big bubble that escapes from the large chamber of the air gun. The small bubble escapes through a small nozzle that has a diameter of the order of 1–2 mm. This is the main explanation for this difference in growing velocity between the two air bubbles. These two bubbles probably merge into one after 2 ms. The next question is whether we can detect the acoustic signal generated by cavities collapsing close to the air gun, at a distance of 60 m below the gun.

ACOUSTIC SIGNALS FROM SINGLE AIR GUNS

Figure 5a shows recorded acoustic signals for three shots representing a single 70 in^3 air gun, a single 300 in^3 air gun, and a cluster of two 300 in^3 air guns. To convert from bar-m to micropascal at 1 m, a multiplication by 10^{11} is needed. We notice that the cluster has a maximum peak that is almost double that of the single gun. Furthermore, we notice that there are small ripples on all signatures, prior to and during the main peak signal. Some of these ripples are high-frequency signals created by the gun, and some are background high-frequency noise. This issue will be further addressed in later sections. The smallest gun (70 in^3) is a slightly different type (Bolt 1900 C) than the larger guns (Bolt 1500 C). In this figure, the closest shots (with respect to the hydrophone) have been chosen and it is assumed that the distance from the source to the seabed hydrophone is 60 m for all shots. As discussed above, there might be a slight variation in this distance because the surface position for the nearest shot might vary by up to 15 m. To convert the signals to bar-m, we have multiplied the recorded signals by 60. Typical relative errors in amplitudes caused by this inaccuracy might be up to 3%. The timing of the maxima for each shot is also somewhat random (5–10 ms spread), and these variations have been adjusted for in Figure 5 so that the rise of the main peak is aligned for various shots.

A detailed comparison of the shoulder signal (the signal prior to the main peak) is displayed in Figure 5b. We notice that the length of this signal is significantly longer for the 300 in^3 air gun (44–48 ms) compared to that for the 70 in^3 air gun (46–48 ms). This might be due to the fact that the two guns are of different types (Bolt 1500 C and 1900 C). The volume of the upper chamber for the larger air gun (300 in^3, 1500 C) is larger than that of the small air gun; hence, the length of this shoulder signal is longer. This interpretation assumes that the shoulder signal is partly created by the small air bubble that is released prior to the main peak (shown by a yellow arrow in Figure 4). Furthermore, we note that the average amplitude level of the shoulder signal is nearly doubled for the cluster signal (red line shown in Figure 5) compared to the single 300 in^3 air gun (black line shown in Figure 5). The 70 in^3 shoulder signal is weaker than that for the 300 in^3 air gun. Again, this is interpreted to be caused by the larger upper chamber volume for the larger gun. The physical mechanism behind the shoulder signal can be multifold. First, the escape of air from the upper chamber (or the top housing) creates an acoustic signal (similar to when the air is released from the large, lower gun chamber). The escape of this air from the upper chamber is shown clearly in Figure 4a (marked by a yellow arrow). This tiny air bubble remains visible throughout Figure 4b–4d; therefore, it is reasonable to assume that this minibubble exists for several milliseconds and will produce a weak acoustic signal. Second, as discussed in the previous section,

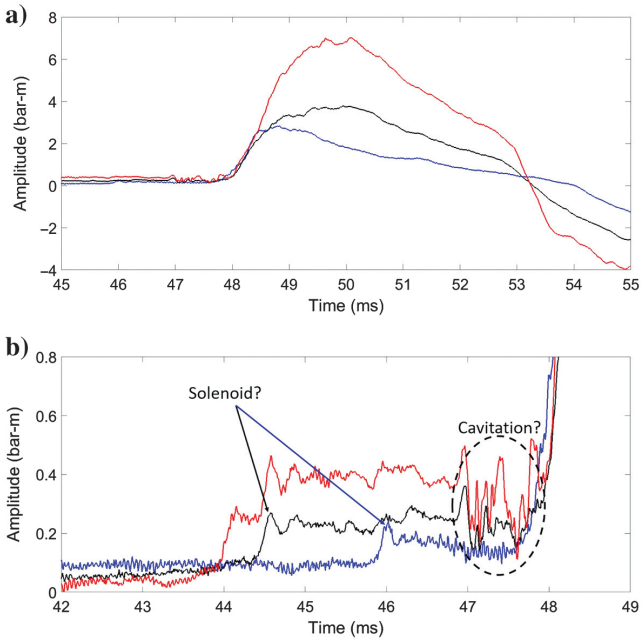

Figure 5. (a) Unfiltered signatures of a single 70 in^3 air gun (blue line), a single 300 in^3 air gun (black line), and a cluster of two 300 in^3 air guns (red line). (b) Portion of (a) magnified to show the shoulder signal (44–48 ms). Notice that the shoulder signal is longer for the 300 in^3 air gun(s) compared to the 70 in^3 air gun.

water vapor cavities that are produced due to rapid water movements close to the air gun will collapse and create high-frequency signals. Other effects that might contribute to the shoulder signal are the solenoid (the electric trigger mechanism for the air gun), the movement of the shuttle, and vibrations caused by the shuttle movement.

There is one common feature for all three signals shown in Figure 5b: the high-frequency signal that occurs between 47 and 48 ms. We think this signal represents small cavities collapsing close to the air-gun ports (such as those shown in Figure 4). Because these cavities are small, they will collapse within a fraction of a millisecond (equation 4); therefore, they will essentially "live" as long as the bubble velocity is above a certain threshold. Again, we observe that the magnitude of this potential cavitation signal is higher for larger guns. It is indeed very difficult to prove that this signal is caused by collapsing cavities; therefore, we use the term "potential cavitation." One way to further strengthen this hypothesis is to apply a high-pass filter to the data and see if the very high frequencies remain. It is typical for cavitation signals that they show a strong high-frequency content. This is shown in Figure 6, where a 30 kHz high-pass filter has been applied, followed by taking the absolute value and a mild smoothing filter. All signals show a distinct increase at approximately 47 ms, more pronounced for the larger gun (black line) and the cluster (red line) than for the small gun (blue line). We also note that the main peak for this high-frequency signal appears prior to the main peak for the unfiltered signatures. For the 70 in^3 gun, the main peak occurs at 48.5 ms; for the 300 in^3 gun, it is at 49.5 ms (Figure 5). For the high-pass-filtered data shown in Figure 6, these maxima occur approximately 2 ms earlier. Furthermore, we note that all three curves decay after the maximum, similar to the modeled bubble wall velocity shown in Figure 2b. All of these observations support the hypothesis that the signal between 47 and 48 ms observed in Figure 5 is caused primarily by cavitation. It should be stressed that this cavitation signal continues after 48 ms because we observe high-frequency signals above the background noise level in the time interval between 47 and 51 ms (Figure 6). We think that the contribution from the solenoid signal is not the main cause for the high-frequency signal observed within the time interval from 47 to 48 ms because the solenoid signal (which is the trigger for the air gun) should be the first acoustic signal to be observed, which in our case means the time interval between 44 and 47 ms. Hence, our interpretation of Figure 5b is that this first part (approximately 3 ms) of the air-gun signal is caused by the solenoid, the minibubble (Figure 4), and water being pushed through the ports (Figure 4).

Furthermore, we observe from Figure 5b that the interpreted cavitation signal (marked by a dashed ellipse) is significantly weaker for the 70 in^3 gun compared to the 300 in^3 gun. However, for the first peak of the shoulder signal, we observe approximately the same amplitude levels for the 70 and 300 in^3 guns (the peaks marked by the black and blue arrows, respectively). Hence, we interpret the very first peak of the air-gun signal as dominated by the solenoid, and the latter part of the shoulder signal contains a significant amount of high-frequency cavitation signal (Figure 6).

Another interesting observation that can be made from Figure 5b is that the shoulder signal of the clustered air guns (red line) increases stepwise: The first step occurs at 44.0 ms, and the next step occurs at 44.4 ms. This probably is caused by the firing time delay of 0.4 ms between the two guns in the cluster. This is reinforced by the fact that the shoulder signal of the cluster array is two times stronger than that of the single gun. After high-pass filtering (Figure 6), we also observe a small time shift (0.2–0.3 ms) between the single gun (black line) and the cluster (red line).

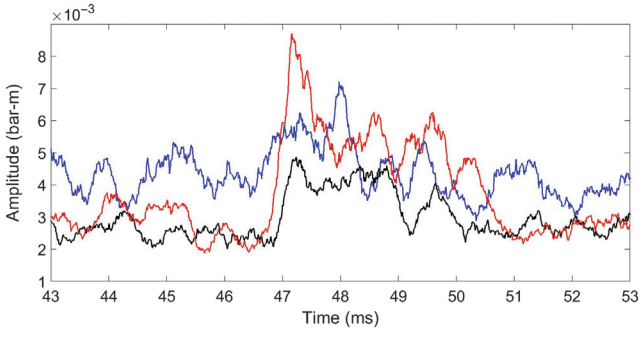

Figure 6. High-pass-filtered signatures (30 kHz filter), followed by the absolute value and smoothing of a single 70 in^3 air gun (blue line), a single 300 in^3 air gun (black line), and a cluster of two 300 in^3 air guns (red line). Notice that there is a significant increase in the high-frequency signal at approximately 47 ms for all signatures.

THE ECHO SOUNDER SIGNAL AND THE CAVITATION SIGNAL

The seismic vessel uses an echo sounder with a 20 kHz dominant frequency. This signal is prominent if we apply a band-pass filter (17.5–22.5 kHz) centered around the dominant frequency (Figure 7). We observe a periodic signal every 8 ms (approximately). However, the signal at 47 ms (marked by the blue arrow) is not caused by the echo sounder and is interpreted as cavitation signal from the air gun. Because the echo sounder signal definitely is a high-frequency signal, we should try to isolate it as much as possible in the analysis. Figure 8 demonstrates how the echo sounder signal becomes more and more prominent as the frequency content of the recorded signal is increased. However, the interpreted cavitation signal at approximately 47 ms is prominent for all frequencies and does not coincide with the echo sounder signal (Figure 7b). This cavitation signal is enhanced further if several shots are stacked together prior to the analysis, as shown in Figure 9 where four shots from the single 300 in^3 air gun have been aligned and then stacked prior to application of a 36–60 kHz band-pass filter. The stacking procedure helps because the echo sounder signals will arrive at random times when different shots are stacked. When the 55 kHz

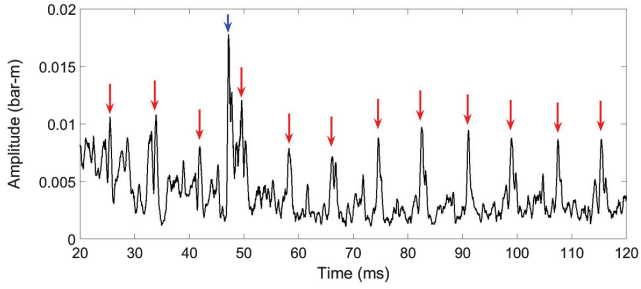

Figure 7. One shot record filtered with a 17.5–22.5 kHz band-pass filter. The regular peaks (the interval is approximately 8 ms) are the echo sounder signal. Note that the peak at 47 ms (marked by the blue arrow) is *not* caused by the echo sounder, but the clustered air guns in this case (corresponding to the red peak shown in Figure 6).

high-pass-filtered data (red curve shown in Figure 9b) is compared to the modeled velocity curve shown in Figure 2, we observe some similarities that may be used as a guide for a qualitative interpretation: As the air is pushed out of the air gun, the water velocity close to the ports reaches a maximum. At this maximum, many cavities are created close to the gun, and they collapse almost instantaneously. As the velocity decreases, the number of cavities created decreases until the velocity is less than the critical velocity (equation 4). The width of the cavitation signal shown in Figure 9b is approximately 2 ms. From the modeled velocity curve shown in Figure 2, this would correspond to a critical velocity of 45 m/s. We know that Figure 2 is not correct (it assumes spherical symmetry; it does not include the air throttling through the ports, etc.), so this number should only be used as an indication. It is indeed possible that the 55 kHz signal shown in Figure 9 is caused by cavitation.

COMPARING SIGNATURES FROM A SINGLE GUN AND A 30-GUN ARRAY

Figure 10 (from Landrø et al., 2016) shows a comparison between a 300 in^3 single air gun and a full array (2730 in^3, 30 guns in total). We note that the acoustic signal produced by the full array is significantly stronger (approximately 8.3 times) compared to the single 300 in^3 gun. From the high-pass-filtered data (30 kHz high-pass filter), we again observe a peak that occurs prior to the main peak of the signature, which is interpreted as being caused by small cavities collapsing close to the gun ports (shown in Figure 4). For the single gun, this event occurs as a clear peak. For the full array, we notice a more "bumpy" signal, indicating that various guns in the full array create cavities at different times depending on individual variation in firing times for the 30 guns in the array.

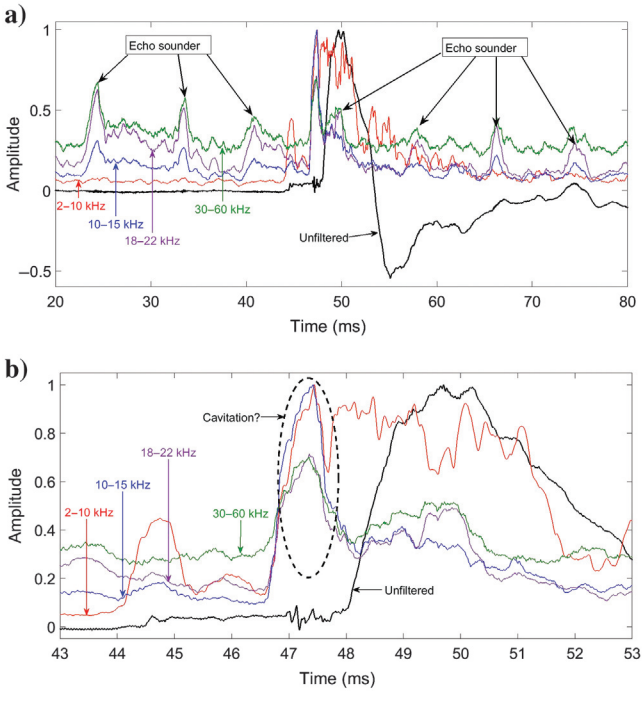

Figure 8. (a) Signature of the 300 cubic signatures filtered with various filters: No filter (black), 2–10 (red), 10–15 (blue), 18–22 (purple), and 30–60 kHz. The dominant frequency of the echo sounder is 20 kHz; hence, we see the regular peaks (at an approximately 8 ms interval) on the purple curve. Notice that the signal prior to the main peak is observed for ALL frequencies (see the magnified version below). Scaling applied to the various curves: 2–10 kHz: 82; 10–15 kHz: 185; 18–22 kHz: 269, and 30–60 kHz: 478. (b) Magnified version of the same figure.

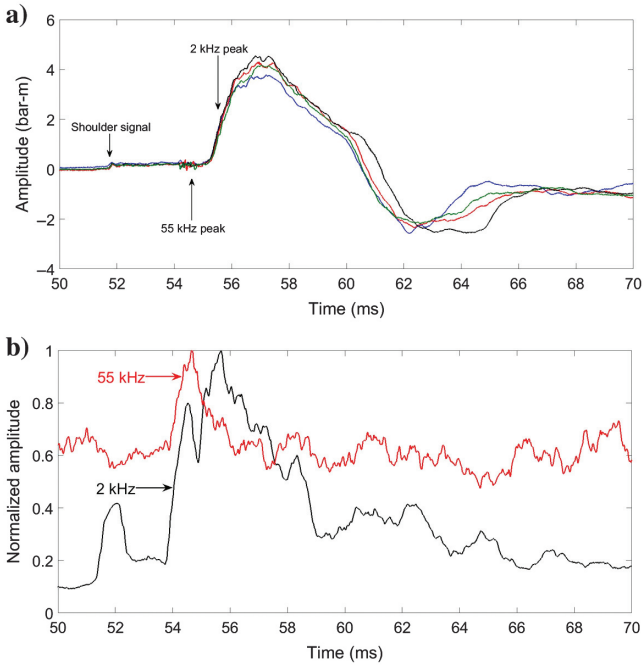

Figure 9. (a) Four shots of a single 300 in^3 air gun. (b) Stack of the four shots after application of a 2 (black curve) and a 55 kHz (red curve) high-pass filter. The filtering process is followed by the absolute value (of each time sample) and a gentle smoother.

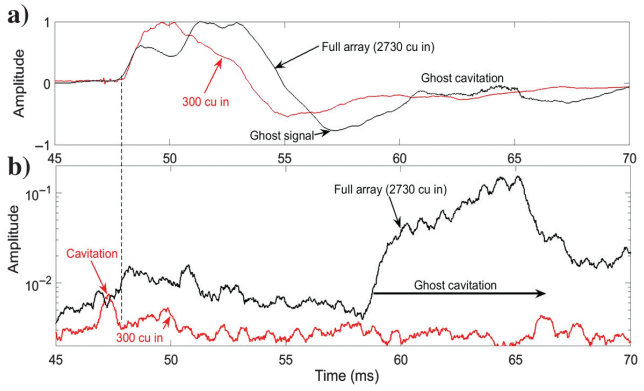

Figure 10. (a) Recorded far-field signals of a full array (black) and a 300 in^3 single air gun (red). The data have been normalized prior to plotting (the maximum amplitude of the full array is 8.3 times that of the single gun). (b) The same data after applying a 30 kHz high-pass filter, absolute value, and smoothing. Notice that cavitation signals are observed prior to the main peak for the single gun (marked by the red arrow), and after the ghost signal for the full array, denoted as ghost cavitation. The ghost cavitation signal is approximately 10 times stronger than the high-frequency signal observed approximately 50 ms for the full array (figure from Landrø et al. 2016).

DOI:10.1190/geo2019-0768.1

We also notice that the primary peak signal of the full array (black line shown in Figure 10a) actually is composed of three individual peaks. These three peaks might be due to slight firing time delays between the three subarrays in the array. The size of the array is 12×15 m, yielding a diagonal of 19 m. For a hydrophone located 60 m away in the vertical direction, this might cause a maximum possible difference in traveltime of approximately 2 ms. Therefore, the spread of the maximum peak of the full array might be caused by a combination of variations in gun firing time delays and small traveltime differences due to the areal spread of the array. Both these effects, therefore, might explain why we observe this bumpy behavior of the high-frequency cavitation signal occurring from approximately 47 to 54 ms for the full array (black curve shown in Figure 10b); this high-frequency signal is interpreted as being composed of individual cavities collapsing close to the gun ports.

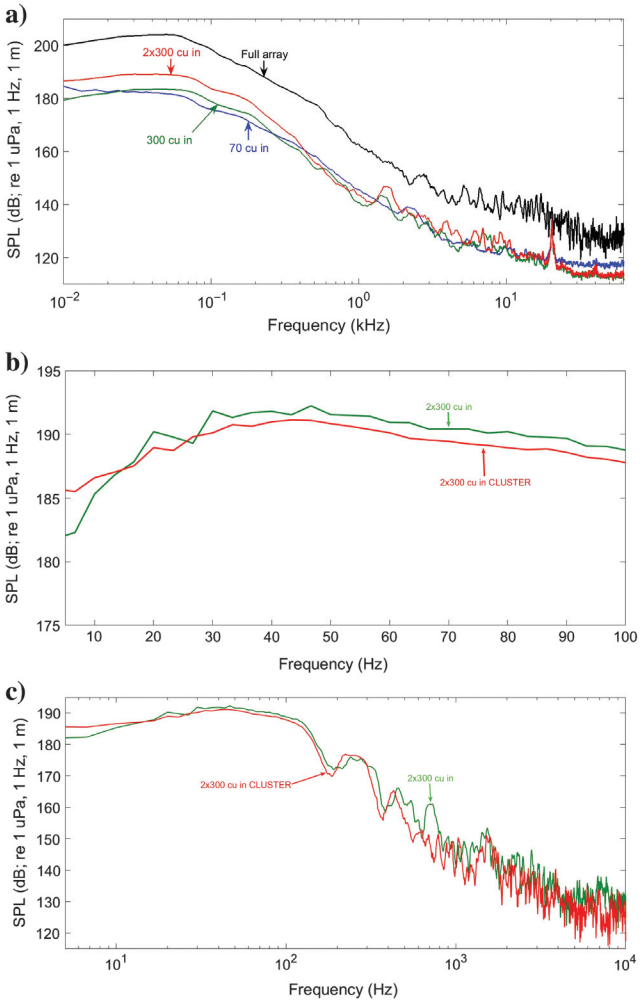

Figure 11. (a) Amplitude spectra in dB for the full array (black line), 70 in^3 air gun (blue line), 300 in^3 air gun (green line), and the 2×300 in^3 cluster (red line). The peak at approximately 20 kHz for the three latter curves is caused by the echo sounder of the vessel. Notice that the difference between the full array and the single guns is of the order of 20 dB for frequencies between 100 Hz and 20 kHz. (b) Amplitude spectra of the 300 in^3 air gun multiplied by 2 (green line) and the 2×300 in^3 cluster (red line). Notice that the cluster generates slightly more low frequencies (below 15 Hz). The recording length is 0.3 s. (c) Amplitude spectra of the 300 in^3 air gun multiplied by 2 (green line) and the 2×300 in^3 cluster (red line). Notice that the cluster generates slightly more low frequencies (below 15 Hz). The recording length is 0.3 s.

However, the biggest difference between high-pass-filtered data for the full array and the single gun is what occurs after 58 ms (Figure 10b). A strong high-frequency signal gradually builds up to a maximum occurring at approximately 65 ms, followed by a sudden decrease. This effect has been described previously by Landrø et al. (2011), and it is denoted as ghost cavitation in Figure 10. We clearly see that it occurs after the strong negative signal at approximately 57 ms. It is assumed that the collective effect of ghost signals from 30 individual guns arriving at approximately the same time (57 ms) and occurring at specific locations (above the mid-array, for instance) is sufficiently strong to lower the absolute pressure in the water close to zero, creating water vapor cavities. It is reasonable to assume that these cavities might be larger in size; hence, the collapse time (see equation 5) will be larger compared to the smaller cavities that collapse at the gun itself. The magnitude of the ghost cavitation signal is approximately 10 times larger than the high-frequency signal associated with the main peak of the signature. The acoustic stimulation of cavities has been studied by numerous researchers. One early example is performed by Harrison (1952). He uses a venture nozzle to generate cavities by high-speed motion of water from the nozzle (very similar to what we claim is the mechanism behind the cavities observed in Figure 4 in this paper). Plesset and Ellis (1955) demonstrate some years later that it is possible to create cavities by acoustic stimulation.

Figure 11a shows a broadband comparison (10 Hz to 62.5 kHz) of the amplitude spectra for the small air gun (70 in^3), the single 300 in^3 air gun, the cluster, and the full array. We notice that the full array is approximately 20 dB stronger than the other guns for the frequency range from 100 Hz up to 20 kHz. For frequencies between 20 and 60 kHz, the difference is somewhat less.

Figure 11b and 11c shows a comparison between two individual 300 in^3 air-gun signals added together to one cluster of two 300 in^3 air guns. As expected, the sum of the individual signals is slightly stronger (0.9 dB) than the cluster for frequencies greater than 15–20 Hz. However, for lower frequencies, we notice that the cluster signal is slightly stronger than that of the two separate guns (3.3 dB). Hopperstad et al. (2012) point out that a hypercluster gives more low frequencies for the same quantity of air used. Their measurements show that the low-frequency peak changed from approximately 9 Hz for individual guns to 5 Hz for a hypercluster with the same total volume (1680 in^3). When these guns are organized in a huge hypercluster, the low-frequency peak drops to 5 Hz, a major shift toward lower frequencies. A simple intuitive explanation for both of these observations is that clusters create a bigger bubble leading to lower acoustic frequencies being generated. The same effect is observed in Landrø et al. (2011), where the low-frequency peak is shifted toward lower frequencies as the source depth is reduced. Reducing the source depth is equivalent to increasing the maximum bubble radius, hence generating more low frequencies.

For very low frequencies (close to 10 Hz), we note that the curve for the smallest gun (70 in^3) crosses that of the larger gun (300 in^3) in Figure 11a. This crossover might be associated with the different bubble time period for the two signals. The 70 in^3 gun has a bubble time period of 70 ms, corresponding to a resonance frequency of 14.3 Hz, whereas the 300 in^3 gun has a bubble time period of 120 ms, corresponding to 8.3 Hz. Hence, the smaller gun will have

the maximum caused by the bubble oscillation at a frequency slightly greater than 10 Hz, whereas the bigger gun will have the maximum at less than 10 Hz. Another cause may be related to varying noise level between the shot series for the different gun configurations. Figure 12 shows noise records (taken from 30 ms prior to the actual firing of the source) for the four source configurations shown in Figure 11. We note that the noise record corresponding to the 70 in^3 air gun is above the other noise records, especially at the low-frequency end. A comparison with a 1/f attenuation also is shown in this figure, and we note that the decay is actually 1/f for frequencies between 10 Hz and 10 kHz. Above 10 kHz, the influence of the echo sounder signal is dominating. Figure 13 shows a comparison between the amplitude spectra of the nearest and furthest shot for the smallest air gun and the full array. We notice that the amplitude strength is practically equal for frequencies greater than 10 kHz for the single gun, whereas the full array spectral difference reaches a maximum at approximately 10–15 kHz and then slightly decreases. At the echo sounder frequency (20 kHz), we note that there is a significant difference for the single gun spectrum (Figure 13). Again, this difference is attributed primarily to the strong ghost cavitation signal for the full array (which is stronger the nearer the source is). For the single gun, the cavitation signal is much weaker, and therefore it is drowning in the background high-frequency noise.

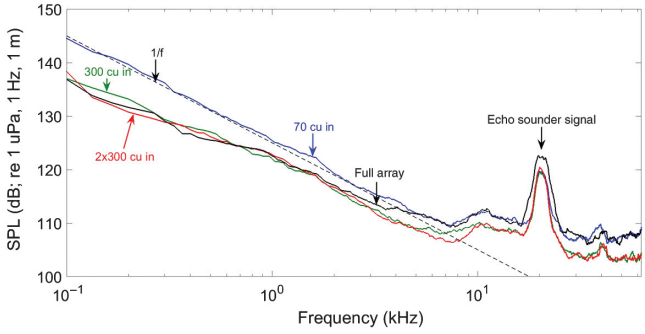

Figure 12. Noise spectra for the four shots depicted in Figure 11. A window of 30 ms prior to the gun firing time is used for the analysis. We notice that the noise level is greater prior to the firing of the 70 in^3 gun (blue line) compared to the others. We notice the characteristic peak of the echo sounder signal at 20 kHz. The slope of this noise corresponds approximately to $1/f$ attenuation between 100 Hz and 7 kHz.

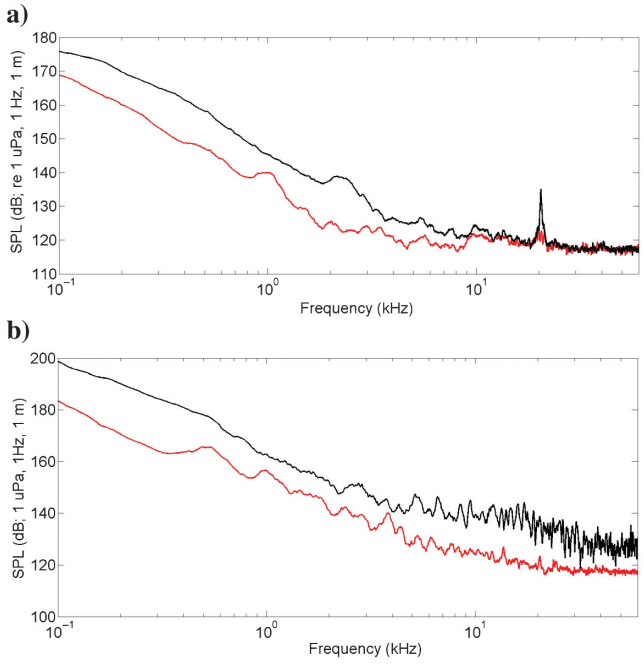

Figure 13. Comparison of the nearest (black lines) and furthest (red lines) shots for the (a) single 70 in^3 air gun and (b) full array. Notice the significant differences between the two sources, especially for frequencies above 10 kHz.

Another way to demonstrate the significance of the ghost cavitation effect is to stack the signal recorded from the cluster array five times. The volume of the cluster array is 600 in^3; by adding it five times and introducing random firing time delays between each of the five elements, a realistic signal simulating the effect of adding five clustered sources together (without accounting for the ghost cavitation effect) is achieved. The total volume of the full array is 2730 in^3, which is slightly less than five times 600 in^3. In Figure 14, we clearly see that, although the strength of this synthetic 3000 in^3 array is the same for low frequencies (less than 20–30 Hz), there is a significant gap between the full array and the 3000 in^3 simulated result for frequencies above 100 Hz. It should be noted that some of the differences between the two arrays are not caused entirely by the ghost cavitation effect because a more broadband frequency signal is obtained by using different source volumes. This is especially true for the frequency band between 20 and 100 Hz, where we observe that the full array has a better response compared to the synthetic array generated by summing the clustered air gun five times.

This paper discusses conventional Bolt air guns only. Details for other air-gun types might be different, especially related to the shoulder signal for individual air guns. Different designs of the port openings and release mechanisms will give different acoustic signals. For the ghost cavitation effects discussed for large and compact arrays, however, this effect is only dependent on the peak signal created by the sum of all of the guns, and therefore it will occur, regardless of the gun type used in the array. The amount

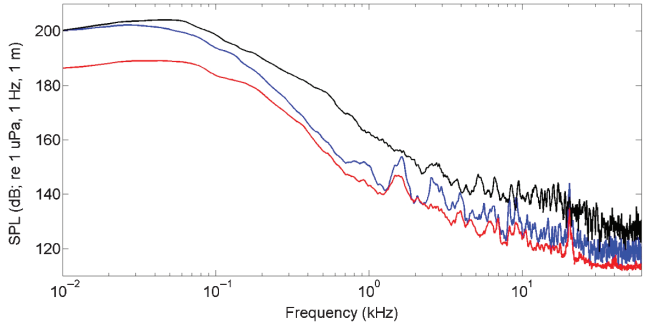

Figure 14. Amplitude spectrum of the full array (black) and the two-gun cluster (red). The blue line represents the two-gun cluster signal being summed five times using a random time delay (1–3 ms) between the five "shots" prior to summation. Notice that the "stacked" cluster array has similar amplitudes compared to the full array for frequencies less than 30 Hz. For higher frequencies, the discrepancy between the two curves increases up to 20 kHz.

of ghost cavitation might vary, of course, depending on the peak signal strength generated by each individual gun.

CONCLUSION

High-speed photographs of a small air gun in a water tank show small bubbles attached to the gun itself that are interpreted as cavities. Simple modeling of the air being released from an air gun into the surrounding water shows that velocities might be well above the critical velocity for cavity creation. A maximum water velocity of approximately 50 m/s is found by comparing two adjacent photos from the initial stages after the air gun has been fired. Recorded underwater acoustic signals, measured 60 m vertically below the air-gun source, show a high-frequency part (2–60 kHz) arriving prior to the main peak, which is interpreted as being caused by collapsing cavities close to the gun. When the full array (30 air guns) is fired, an additional cavitation signal that is much stronger than the cavitation signals being produced by individual air guns is observed. This signal occurs at a later stage (after the ghost signal) and is referred to as ghost cavitation signal.

ACKNOWLEDGMENTS

Martin Landrø thanks the Norwegian Research Council for financial support to the GAMES consortium at the Research Council of Norway (grant no. 294404) and to the ARCEx (Research Centre for Arctic Petroleum Exploration, grant no. 228107). Two anonymous reviewers and two editors, Carlos Torres-Verdin and Jeffrey Shragge, are thanked for their several constructive suggestions and corrections that improved the paper.

DATA AND MATERIALS AVAILABILITY

Data associated with this research are confidential and cannot be released.

REFERENCES

Abma, R., and A. Ross, 2013, Popcorn shooting: Sparse inversion and the distribution of airgun array energy over time: 83rd Annual International Meeting, SEG, Expanded Abstracts, 31–35, doi: 10.1190/segam2013-0592.1.

Amundsen, A., and M. Landrø, 2010, Seismic sources — Part 5: The hearing of marine mammals: GeoExpro, **7**, 64–66.

Amundsen, A., and M. Landrø, 2011a, Seismic sources — Part 6: High frequency signals from air guns: GeoExpro, **8**, 69–71.

Amundsen, A., and M. Landrø, 2011b, Seismic sources — Part 7: Fish are big talkers: GeoExpro, **8**, 64–67.

Barker, D., and M. Landrø, 2014, An alternative method for modeling close-range interactions between air guns: Geophysics, **79**, no. 2, P1–P7, doi: 10.1190/geo2013-0141.1.

Breitzke, M., O. Boebel, S. El Naggar, W. Jokat, and B. Werner, 2008, Broad-band calibration of marine seismic sources used by R/V Polarstern for academic research in polar regions: Geophysical Journal International, **174**, 505–524, doi: 10.1111/j.1365-246X.2008.03831.x.

Christie, P., R. Laws, E. Kragh, P. Nevill, and K. Davis, 2019, Noise characteristics of near-gun hydrophone data used in imaging: 81st Annual International Conference and Exhibition, EAGE, Extended Abstracts, Th_P05_06.

Coste, E., D. Gerez, H. Groenaas, O. P. Larsen, M. Wolfstirn, J. F. Hopperstad, R. Laws, J. Norton, and M. Padula, 2014, Attenuated high-frequency emission from a new design of air-gun: 84th Annual International Meeting, SEG, Expanded Abstracts, 132–137, doi: 10.1190/segam2014-0445.1.

Dragoset, B., 2000, Introduction to air guns and air gun arrays: The Leading Edge, **19**, 892–897, doi: 10.1190/1.1438741.

Goold, J. C., and P. J. Fish, 1998, Broadband spectra of seismic survey air-gun emissions, with reference to dolphin auditory thresholds: The Journal of the Acoustical Society of America, **103**, 2177–2184, doi: 10.1121/1.421363.

Groenaas, H. S. G., S. A. Frivik, A. S. Melboe, and M. Svendsen, 2011, A novel marine mammal monitoring system utilizing the seismic streamer spread: 73rd Annual International Conference and Exhibition, EAGE, Extended Abstracts, D047.

Harrison, M., 1952, An experimental study of single bubble cavitation noise: The Journal of the Acoustical Society of America, **24**, 776–782, doi: 10.1121/1.1906978.

Hegna, S., T. Klüver, and L. Lima, 2018, Making the transition from discrete shot records to continuous wavefields — Methodology: 80th Annual International Conference and Exhibition, EAGE, Extended Abstracts, We A10 03.

Hopperstad, J. F., R. Laws, and E. Kragh, 2012, Hypercluster of air guns — More low frequencies for the same quantity of air: 74th Annual International Conference and Exhibition, EAGE, Extended Abstracts, Z011.

Khodabandeloo, B., and M. Landrø, 2018, Acoustically induced cavity cloud generated by air-gun arrays — Comparing video recordings and acoustic data to modeling: The Journal of the Acoustical Society of America, **143**, 3383–3393, doi: 10.1121/1.5040490.

Khodabandeloo, B., and M. Landrø, 2019, Characterizing the acoustic properties of the cavity cloud generated close to an air-gun array as a time-dependent effective medium: Geophysical Journal International, **216**, 545–559, doi: 10.1093/gji/ggy449.

Khodabandeloo, B., M. Landrø, and A. Hanssen, 2017, Acoustic generation of underwater cavities — Comparing modeled and measured acoustic signals generated by seismic air gun arrays: The Journal of the Acoustical Society of America, **141**, 2661–2672, doi: 10.1121/1.4979939.

Landrø, M., 1992, Modelling of GI gun signatures: Geophysical Prospecting, **40**, 721–747, doi: 10.1111/j.1365-2478.1992.tb00549.x.

Landrø, M., L. Amundsen, and D. Barker, 2011, High-frequency signals from air-gun arrays: Geophysics, **76**, no. 4, Q19–Q27, doi: 10.1190/1.3590215.

Landrø, M., L. Amundsen, and J. Langhammer, 2013, Repeatability issues of high-frequency signals emitted by air-gun arrays: Geophysics, **78**, no. 6, P19–P27, doi: 10.1190/geo2013-0142.1.

Landrø, M., Y. Ni, and L. Amundsen, 2016, Reducing high-frequency ghost cavitation signals from marine air-gun arrays: Geophysics, **81**, no. 3, P47–P60, doi: 10.1190/geo2015-0112.1.

Landrø, M., G. Zaalberg-Metselaar, B. Owren, and S. Vaage, 1993, Modeling of water-gun signatures: Geophysics, **58**, 101–109, doi: 10.1190/1.1443339.

Langhammer, J., 1994, Experimental studies of energy loss mechanisms in air gun bubble dynamics: Ph.D. thesis, Norwegian University of Science and Technology (NTNU), no. 125.

Langhammer, J., and M. Landrø, 1996, High speed photography of the bubble generated by an air gun: Geophysical Prospecting, **44**, 153–172, doi: 10.1111/j.1365-2478.1996.tb00143.x.

Plesset, M. S., and A. T. Ellis, 1955, On the mechanism of cavitation damage: Transactions of the ASME, **77**, 1055–1064.

Rayleigh, O. M., 1917, On the pressure developed in a liquid during the collapse of a spherical cavity: Philosophical Magazine, **34**, 94–98, doi: 10.1080/14786440808635681.

Southall, B. L., J. J. Finneran, C. Reichmuth, P. E. Nachtigall, D. R. Ketten, A. E. Bowles, W. T. Ellison, D. P. Nowacek, and P. L. Tyack, 2019, Marine mammal noise exposure criteria: Updated scientific recommendations for residual hearing effects: Aquatic Mammals, **45**, 125–232, doi: 10.1578/AM.45.2.2019.125.

Telling, R., S. Grion, S. Denny, and G. Williams, 2019, Source ghost generation: Observations from a dual near-field hydrophone test: First Break, **37**, 31–38, doi: 10.3997/2214-4609.201802110.

Watson, L. M., J. Werpers, and E. M. Dunham, 2019, What controls the initial peak of an air-gun source signature: Geophysics, **84**, no. 2, P27–P45, doi: 10.1190/geo2018-0298.1.

Ziolkowski, A., 1970, A method for calculating the output pressure waveform from an air gun: Geophysical Journal of the Royal Astronomical Society, **21**, 137–161, doi: 10.1111/j.1365-246X.1970.tb01773.x.